

Landslides (2022) 19:1735–1749
 DOI 10.1007/s10346-022-01889-5
 Received: 23 November 2021
 Accepted: 7 April 2022
 Published online: 25 April 2022
 © Springer-Verlag GmbH Germany,
 part of Springer Nature 2022

Xin Liang · Samuele Segoni · Kunlong Yin · Juan Du  · Bo Chai ·
 Veronica Tofani · Nicola Casagli



Characteristics of landslides and debris flows triggered by extreme rainfall in Daoshi Town during the 2019 Typhoon Lekima, Zhejiang Province, China

Abstract Climate change and rapid urban expansion can foster landslide disasters and cause severe damage in areas that are traditionally considered relatively safe from such hazards. In this regard, a recent event in Daoshi Town, China, is a good example that showcases the combined effect of extreme rainfall and urbanization in generating a first-time landslide disaster for a developing community. On 10 August 2019, Typhoon Lekima made its landing in Zhejiang Province, China. It generated a rainstorm close to Daoshi Town, inducing severe and unexpected damage from shallow landslides and debris flows (7 deaths, 25,560 affected and a direct economic loss of 1.5 hundred million dollars). In this region, similar rainfall has never been experienced before, and landslides have seldom been reported in the past. Field investigations and measurements were conducted to identify the landslide distributions, size characteristics, and mobility. A landslide inventory map, including 251 shallow landslides and 82 debris flows, was compiled to study the geological and topographical factors related to widespread failure. The results showed that shallow landslides and debris flows mainly occurred in the north-central part of the study area, in which the base was mainly composed of strongly weathered limestone. The elevation, mean slope, and slope aspect also contributed to the occurrence of landslides. In addition, 32.4% of the disasters were located close to buildings and roads, highlighting a relevant predisposing role played by human activity. This typhoon-bound rainstorm gave rise to a higher triggering condition than the normally required rainfall threshold in the study area. Under this circumstance, landslides were easily triggered and were able to transition into debris flows due to liquefaction. Field observations demonstrate that the erosion of slope toes caused by debris flows also facilitated the occurrence of other shallow landslides. A changing climatic setting is a never-before-experienced phenomenon for the study area. This research improves the understanding of landslide development in the area and prepares basic data and information for further studies and mitigation strategies.

Keywords Shallow landslide · Debris flow · Typhoon Lekima · Extreme rainfall · Landslide characteristics

Introduction

In the coastal areas near the western North Pacific Ocean, typhoons make land almost every hydrological year. As a rapidly rotating storm system, its migration always comes with torrential rain, squalls, and destructive storm surges (Easterling et al. 2000),

and thus induces a series of shallow landslides, debris flows, and other natural hazards, which directly affect millions of people and cause enormous economic loss (Wang et al. 2005; Wu et al. 2014a, b; Abancó et al. 2021). To mitigate risks from typhoons and their secondary hazards, some scholars have obtained the features of typhoons (such as tracks, wind speeds, and typhoon-bound rainfall) through observation and model prediction and developed contingency strategies for multiple hazards in different typhoon scenarios (Oouchi et al. 2006; Mok et al. 2020; Kim et al. 2019). However, powerful typhoons are increasing obviously with global climate change (Webster et al. 2005; Fogarty et al. 2006; Wu et al. 2020), and the accompanying landslides and debris flows triggered by extreme rainfall from the typhoons have become disastrous threats to many northwestern Pacific countries. It is thus necessary to conduct specific investigations and studies on the relationship between typhoon events, extreme rainfall, and their secondary geological hazards.

Increasing evidence shows that typhoon-bound rainfall is the main factor initiating shallow landslides and debris flows in coastal mountain areas (Saito et al. 2014). For instance, Typhoon Namtheun made its landfall on Shikoku Island, Japan, on August 2004 with a corresponding rainfall reaching 120 mm/h, which had a major contribution to the occurrence of numerous long-runout landslides (Wang et al. 2005). Similarly, Typhoon Morakot on August 2009 brought a massive rainstorm of 1890 mm within 77 h. Then, a total of 22,705 landslides were recognized in its striking region, leaving catastrophic destruction and casualties (Wu et al. 2014a; Chen 2016). The extreme precipitation characterized by short-term rainstorms with high intensity could change the internal hydrological distribution and stress equilibrium of the slope and further reduce its stability (Iverson 2000). As rainfall accumulates infiltration, the moisture content of the slope gradually increases, causing groundwater migration and favouring the escalation of pore water pressure (Rosone et al. 2018; Kang et al. 2020; Liang et al. 2021). The increase in unit weight and the reduction in matric suction results in a decrease in the mechanical strength of the soil on the slope (Seboong and Lu 2015). Moreover, the movement of fine particles during groundwater flow could block the seepage paths in the soil, which is also negative to the hydromechanical behaviour of the slope materials (Cui et al. 2019). Carey et al. (2021) found that the liquefaction or slide-flow failure effect caused by transient increases in pore water pressure dominated the generation

of debris flows, thus extending the intensity and scope of the geological hazard.

Many studies point out that the occurrence of shallow landslides and debris flows initiated by extreme rainfall from typhoons has site-specificity and clustered characteristics (Li et al. 2019; Erin et al. 2020; Yang et al. 2020; Abancó et al. 2021). They appeared in the coastal area where typhoons have passed by, usually with a large number of widespread failures in the same rainfall event. However, only a few studies have documented such events or analysed their triggering conditions. Particularly, there are no detailed discussions about the evolutionary characteristics of such regional landslide events in the area, which did not experience prior similar rainfall. From a long-term perspective, it is critical to determine the transformation pattern between landslides and debris flows during a typhoon scenario, which benefits the development of prevention and control measures to mitigate risks from these hazards.

In this study, we investigated a regional landslide event triggered by an extreme rainstorm during Super Typhoon Lekima on 10 August 2019 in Zhejiang Province. As one of the largest typhoons that ever landed in China, it moved on land for 44 h, resulting in 71 deaths and 9.3 billion dollars in damages. We conducted field surveys of 251 shallow landslides and 82 debris flows in Daoshi Town, Linan District, which had never experienced a rainstorm that was intensive as Typhoon Lekima. According to the detailed geological survey, the geological and topographical features of landslides and debris flows were summarized, and the relationships between these two kinds of hazards were discussed.

Study area

Daoshi Town is located in northwestern Zhejiang Province, China, within longitudes $118^{\circ}52'$ – $119^{\circ}01'$ east and latitudes $30^{\circ}12'$ – $30^{\circ}22'$ north (Fig. 1). It covers a total area of 139.1 km^2 , and more than 65.2% of the town is occupied by a mountainous region (Hangzhou Municipal Bureau of Statistics 2017). As shown in Fig. 1c, the area includes flat plains, small hills, and low mountains. The Renli River and Houxi River cross the alluvial plain and divide the study area into three parts. The elevation of the region rises gradually from the river valley plain, varying from 423.3 to 1305.5 m. According to Ren (1991), Daoshi Town experienced two different tectonic events, namely, the Indosinian orogeny during the Triassic and the Yan-shan orogeny in the Late Jurassic. Hence, the geological structure is complex in the study area, and eight main faults are present. The lithology in Daoshi Town mainly consists of tuff, siliceous rock, dolomite, limestone, mudstone, shale, sandstone, clastic rock, and granite (Fig. 2). The Quaternary sediments with various origins overlie the impervious bedrock. The residual soil is relatively thin, with thicknesses of approximately 0.2–3.7 m, and is vulnerable to failure under extreme rainfall conditions.

Daoshi Town is characterized by a subtropical monsoon climate with four distinctive seasons. It has a humid summer and a dry winter. The average annual temperature is 15.9°C , and the average annual relative humidity is 82.0%. Compared with the places on the southeast coast of Zhejiang Province (e.g., Chengnan town in Fig. 3b), Daoshi Town is approximately 325 km away from the East China Sea and experiences

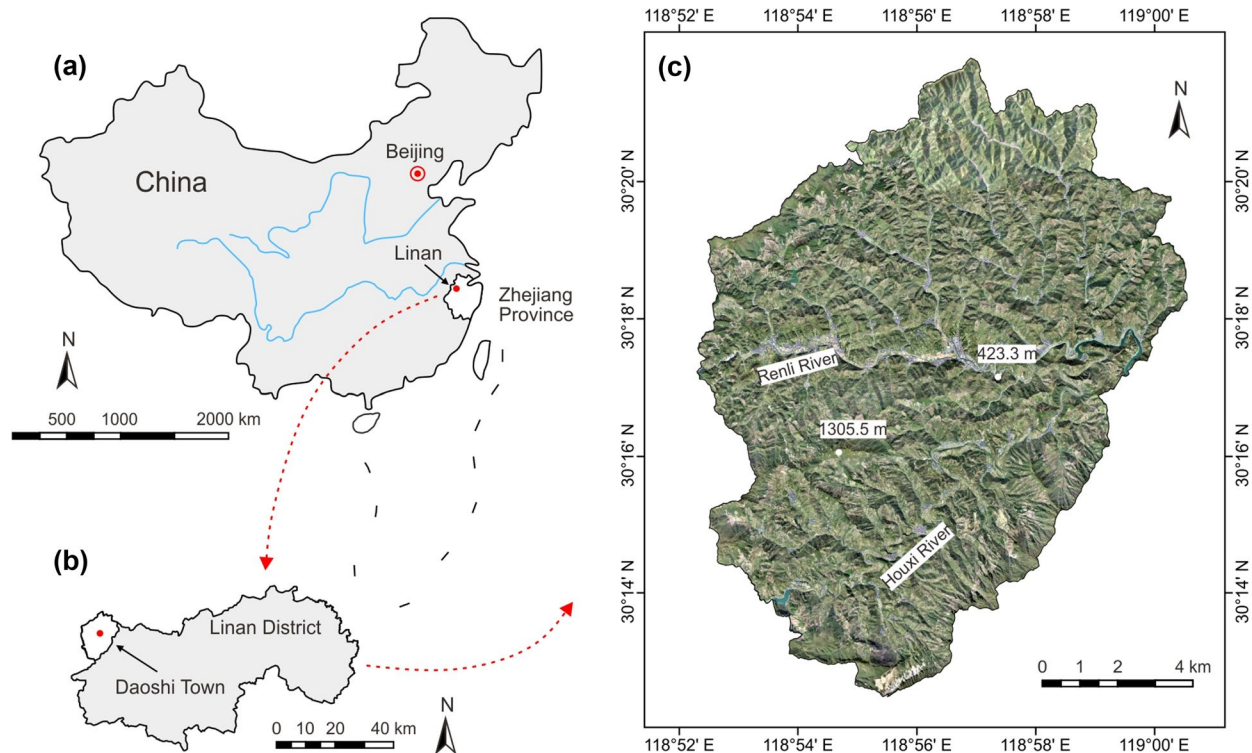
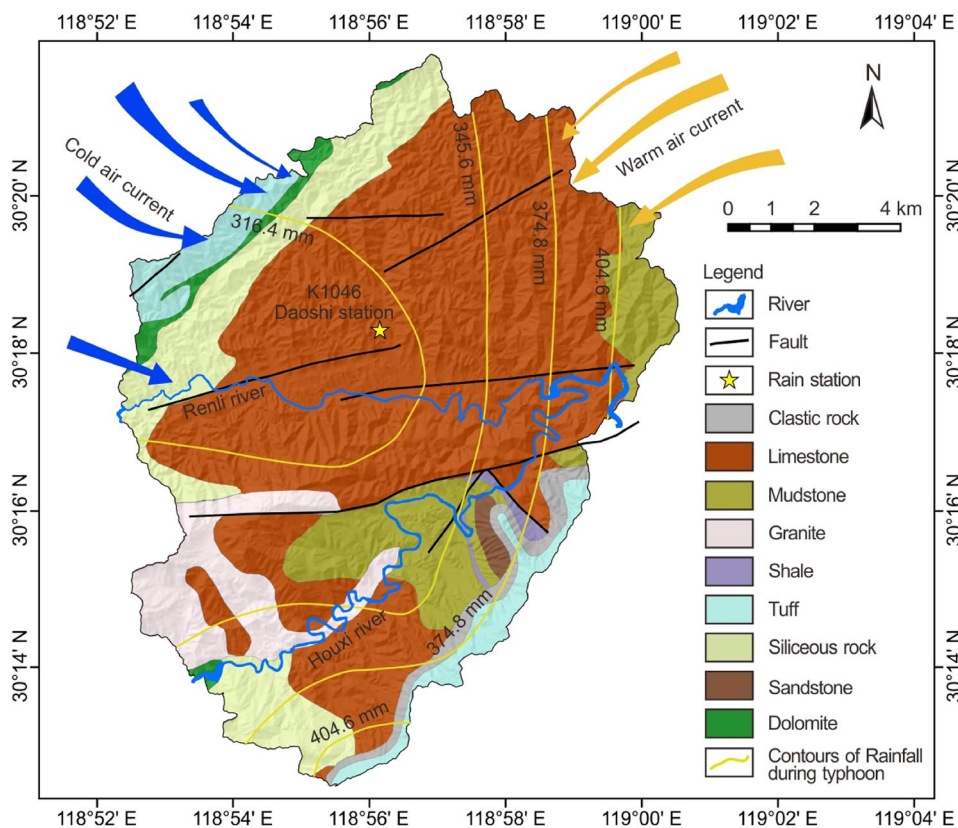


Fig. 1 Location of the study area. (a) Location of the Linan District, Zhejiang Province, China. (b) Site location of Daoshi Town. (c) Satellite image of Daoshi Town

Fig. 2 Geological map of the study area



less influence from typhoons, so the amount and intensity of precipitation are relatively small (Wu et al. 2014b). According to meteorological records from 1971 to 2018, the average annual rainfall is 1586.4 mm, with a maximum monthly average rainfall of 228.5 mm in June. Rainfall is usually concentrated from April to October, which accounts for 75.2% of the annual rainfall. Additionally, the historical geological hazards inventory indicates that

only 14 small landslides existed in the study area before Typhoon Lekima, and no debris flows were reported in the past decades.

Rainfall characteristics during Typhoon Lekima

Super Typhoon Lekima is the third strongest storm that has landed in Zhejiang Province since 1949 in terms of wind speed. It originated from a tropical depression formed in the western Pacific Ocean and gradually shifted to the northwest under the guidance

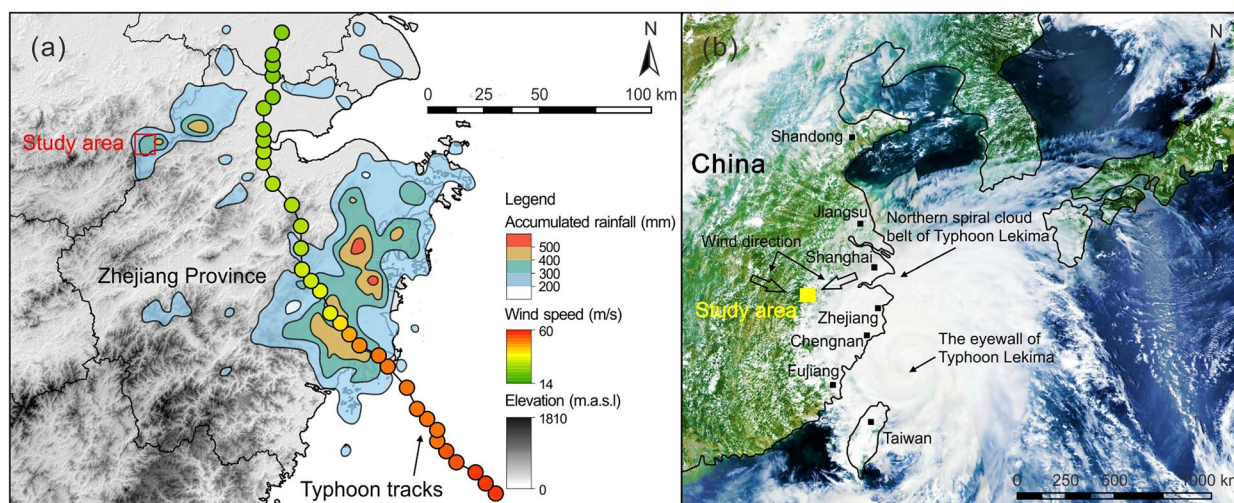


Fig. 3 Characteristics of the Super Typhoon Lekima. (a) Tracks of the Super Typhoon Lekima and accumulated rainfall from 8:00 China Standard Time (CST) on 9 August 2019 to 8:00 CST on 11 August

2019 in Zhejiang Province. (b) Satellite image of Typhoon Lekima at 13:30 CST on 9 August 2019 captured by the Visible Infrared Imaging Radiometer Suite (VIIRS) on the Suomi NPP satellite

of subtropical high pressure (Lou et al. 2020). As shown in Fig. 3, the cyclone made landfall off the coast of Chengnan Town, Wenling City, at 1:45 China Standard Time (CST) on 10 August, with a maximum wind force of 52 m/s near the centre. Then, it left Zhejiang Province and travelled across Eastern China from south to north (Fig. 3a). However, the friction caused by land terrain combined with the loss of heat and moisture sources led to the weakening of the system (Liu et al. 2020). Eventually, it disappeared in the Yellow Sea after 44 h of migration, leaving behind enormous casualties and property loss (a total of 71 deaths and 9.3 billion dollars in economic loss).

Typhoon Lekima hovered around Zhejiang Province for approximately 20 h and brought an extreme rainstorm to the area. A total of 135 national rainfall stations obtained a record that exceeded 90% of their historical maximum daily rainfall, with a further 6 stations breaking their historical records (Lou et al. 2020). Figure 3a shows the spatial distribution of cumulative rainfall from 9 to 11 August 2019 in Zhejiang Province. During the entire typhoon event, three noticeable rainstorm centres were formed in the area. Except for two of them located in the coastal areas near landing sites, a relatively small anomaly was concentrated in the mountainous region close to the study area (Fig. 3a). As analysed by Zheng et al. (2021), the extreme rainfall was related to the long-term mesoscale convective activity in the northern spiral cloud belt of Lekima (Fig. 3b). Moreover, the local topography of the mountains dominated the near-surface circulation of the typhoon, which generated updrafts along the windward slopes and further enhanced the rainfall intensity.

Figure 4 illustrates the temporal evolution of hourly and cumulative rainfall during Typhoon Lekima. According to the records from rain gauge K1046, the rainstorm started at 13:00 CST on 9 August and lasted until 11 August, corresponding with the arrival of the northern spiral rainband of the typhoon (Liu et al. 2020).

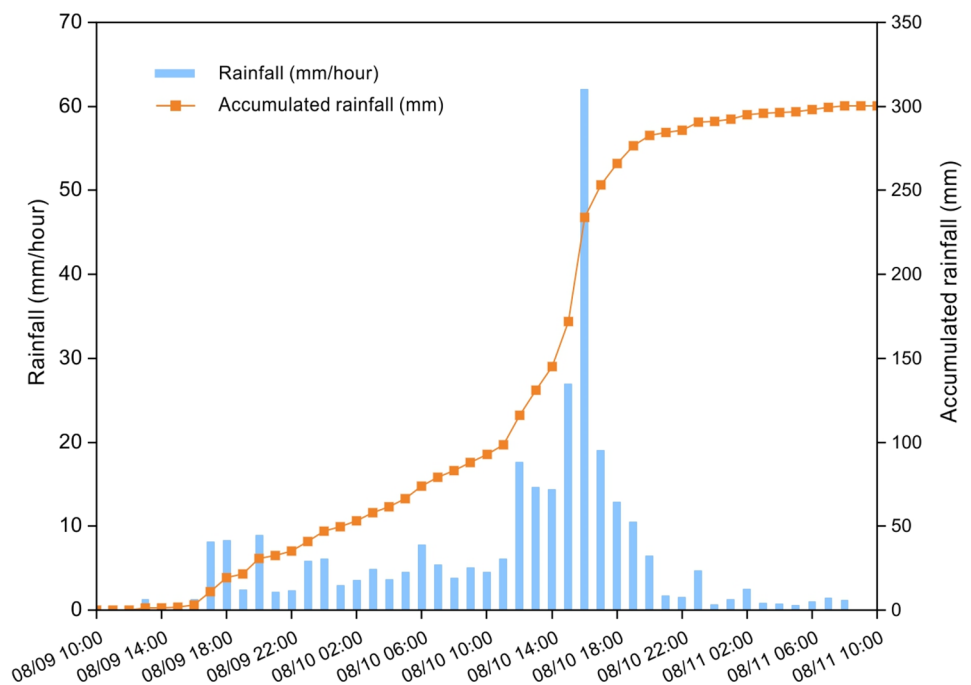
In the beginning, heavy rain of approximately 4 mm/h continued until 11:00 CST on 10 August, with a total amount of 98.7 mm. Then, the rainfall intensity increased dramatically as the eye of the typhoon closed in on the study area. Over the next 8 h, an additional 177.7 mm of precipitation fell in Daoshi Town, resulting in numerous shallow landslides and debris flows. The hydrological statistics with 47 years of rainfall data from 1971 to 2018 indicate that the maximum daily (249.9 mm) and 3-day rainfall (308.5 mm) at Daoshi Town exceeded the historical record, with recurrence intervals of 51 and 108 years, respectively.

Landslides and debris flows in Daoshi Town

Methods

To obtain a complete inventory of geological hazards induced by Typhoon Lekima, field investigations were conducted on August and December 2019. Moreover, remote sensing images from the SuperView-1 satellite were utilized for landslide visual interpretation (Guzzetti et al. 2012). Then, detailed surveys and measurements were undertaken for all vulnerable sites with the references of 1:10,000 geological maps and 1:2000 topographic maps. In particular, unmanned aerial vehicles (UAVs) were employed to reconstruct the three-dimensional digital surface model for some typical shallow landslides and debris flow catchments (Eker et al. 2018). Since the first fieldwork was carried out immediately after the typhoon event, it is possible to recognize some critical features of geohazards. The morphological characteristics, geological structures, and lithologies of landslides and debris flows were determined. For landslides with a distinguishable accumulation area, the runout distance was measured. Moreover, to better reconstruct the mobilization and erosion processes of sediment, the material sources of some debris flows were verified, and erosion traces were identified in drainage channels.

Fig. 4 Rainfall records at Daoshi Town (data from rain gauge K1046 in Fig. 2) from 8:00 CST on 9 August 2019 to 8:00 CST on 11 August 2019



Results

Spatial distribution and size characterization of landslides

According to the classification criteria proposed by Cruden and Varnes (Cruden and Varnes 1996; Hungr et al. 2014), slope failures in the study area can be classified as shallow translational slides and debris flows. Typically, the depths of the sliding surfaces range from 0.2 to 3.7 m. As shown in Fig. 5a, a total of 251 shallow landslides and 82 debris flow basins were identified in the study area. The sliding material is mainly Quaternary sediments accumulated via different geneses. The sizes of landslide scars range from 3.5 to $4.8 \times 10^3 \text{ m}^2$, while their volumes are between 5.2 and $4.0 \times 10^3 \text{ m}^3$. Compared with shallow landslides, debris flows occupy a broader

magnitude. The watershed areas of debris flow basins range from 3.7×10^2 to $7.1 \times 10^5 \text{ m}^2$, and the volumes of accumulated deposits vary between 1.5×10^2 and $2.0 \times 10^4 \text{ m}^3$. Through kernel density analysis, the relative spatial density of geohazard numbers induced by the Typhoon Lekima is shown in Fig. 5b. Most failures are distributed in the mountainous area in the north-central part of Daoshi Town. In addition, a great number of shallow landslides and debris flows are adjacent to roads and houses, accounting for 32.4% of the disasters in the study area (Fig. 6a–e), which halted traffic, damaged buildings, and caused casualties directly during this regional landslide event.

Most landslides triggered by Typhoon Lekima are small in size; 43.8% of slide scars are less than $2.0 \times 10^2 \text{ m}^2$, and 40.2% of debris flow basins are limited to less than $1.0 \times 10^4 \text{ m}^2$. The total area of

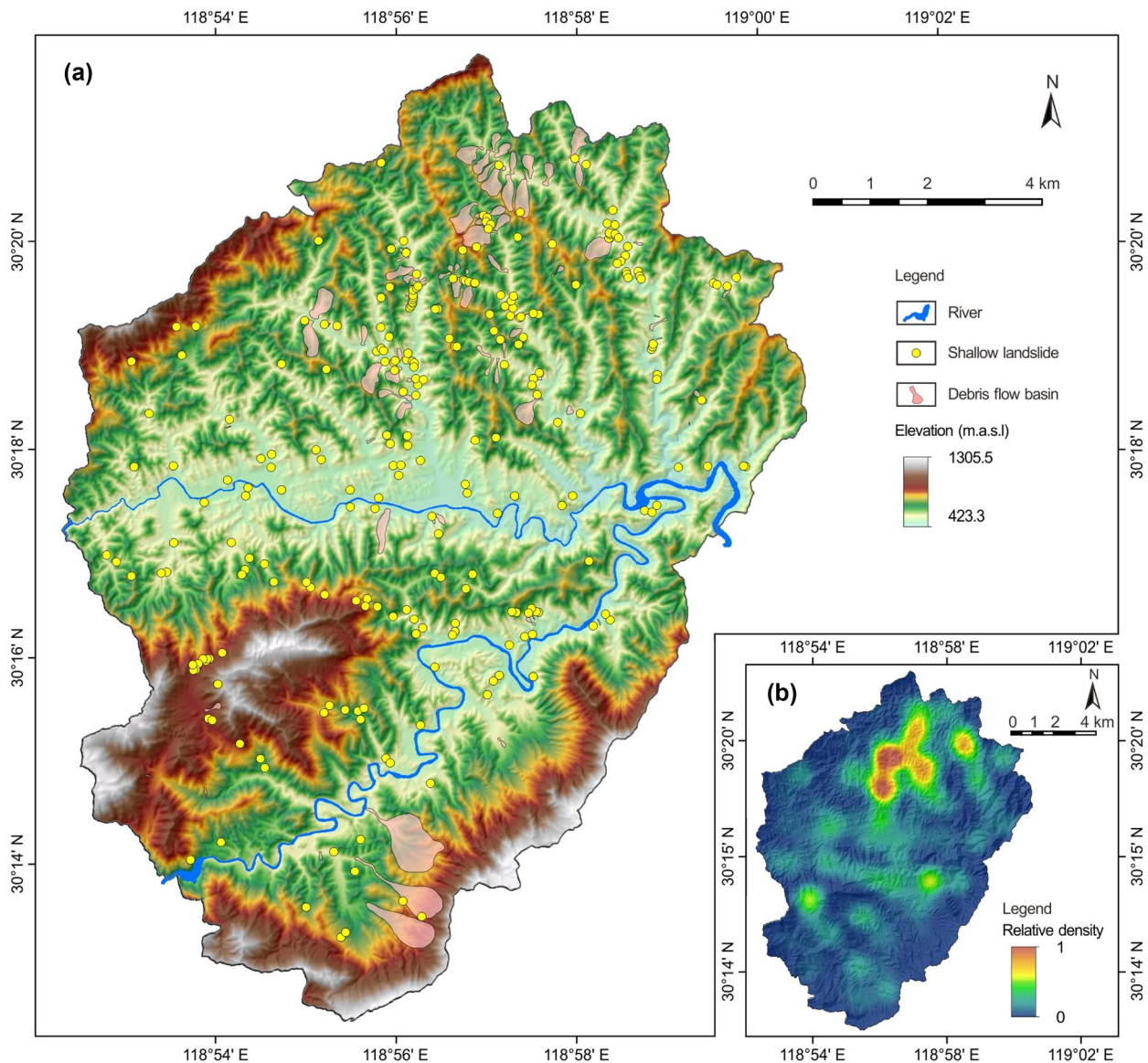


Fig. 5 Location of geohazards in the study area. (a) Spatial distribution of shallow landslides and debris flow basins. (b) Relative density calculated through kernel density analysis

these two kinds of failures is 4.4 km², accounting for 3.2% of Daoshi Town, with average areas of 3.2×10^2 m² and 5.1×10^4 m², respectively. To better understand the size characterization of landslides in the study area, the relationship between the failure magnitude and probability density has been investigated. The probability density is expressed as the ratio of the number of landslides within a specific area range to their total occurrences and corresponding area intervals (Guzzetti et al. 2002). In many regional studies, probability density-area curves of landslides have been proven to have power-law dependence, which is characterized by distinctive turning points (Eeckhaut et al. 2007; Rosi et al. 2018). According to previous field surveys, shallow landslides in Daoshi Town are divided into 20 classes. The related noncumulative density-size distribution is demonstrated in Fig. 7. Landslide areas (A) and the associated probability densities (P) for different blocks are plotted in the cartesian and logarithmic coordinate systems, and the fitted curve is drawn according to an empirical power-law relationship, yielding a correlation coefficient of 0.979. The area of the rollover point is 200 m², indicating that the majority of landslide scars are concentrated between 100 and 200 m² (Fig. 7a). Moreover, points beyond the

rollover have a linear relationship in logarithmic coordinates, with a corresponding correlation coefficient of 0.986 (Fig. 7b). Similar fitting results have been found elsewhere in the world, e.g., in central Italy and California (Guzzetti et al. 2002).

Geological and topographical features

Generally, rugged mountainous terrain is susceptible to landslides, which tend to cluster within a similar geomorphological setting. The studied event provides an opportunity to gain insights into the geological and topographical features that affected the occurrence of landslides in Daoshi Town to understand where similar phenomena could strike in the future. Two quantitative indices, named the landslide number percentage (LSNP) and landslide density (LSD), are introduced to preliminarily evaluate the effect of lithology, elevation, slope angle, and slope aspect on the landslide distribution. The LSNP is obtained by dividing the number of landslides in each classification by the total occurrence. The LSD represents the density of landslides in a particular range and can be expressed as the ratio of the landslide number to the area of the corresponding class. Both of these two indices are available to

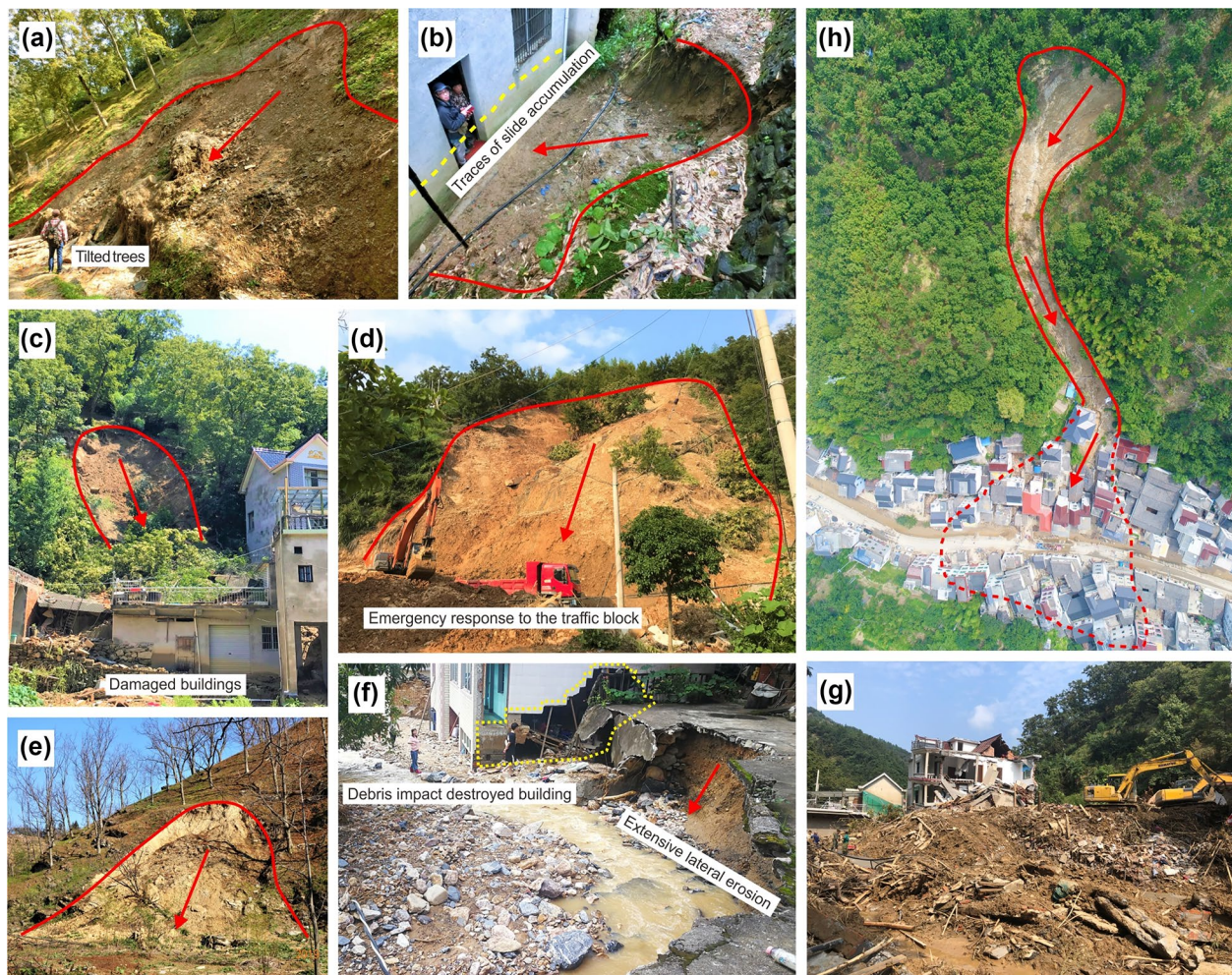
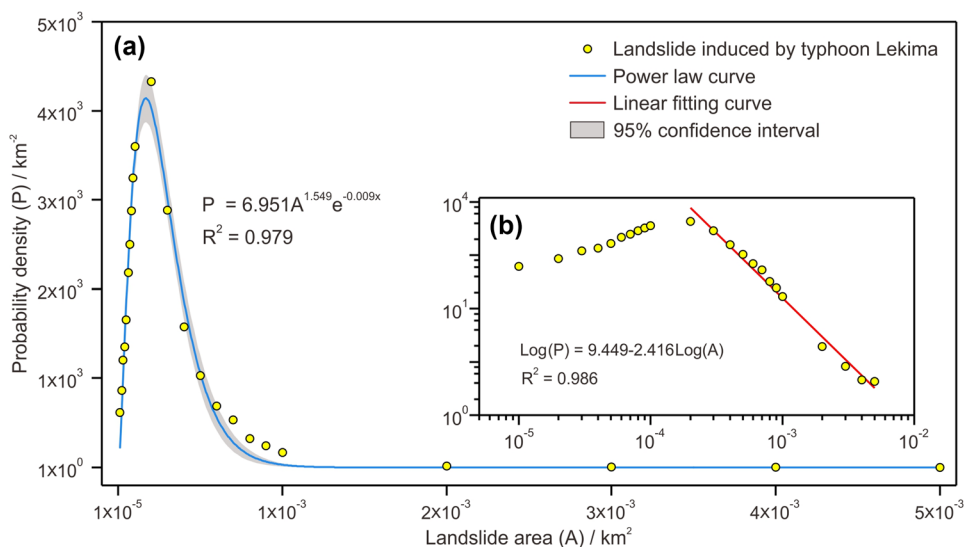


Fig. 6 Field photos of typical shallow landslides and debris flows. (a–e) Sliding in different scenarios. (f–g) Severe damage to buildings and roads. (h) Three-dimensional digital surface model of a small debris flow

Fig. 7 Noncumulative density-size distribution of shallow landslides during Typhoon Lekima in Daoshi Town



distinguish the dominant geological or topographic conditions of landslide distribution.

The relationship between the landslide distribution and involved lithologies is analysed first. Although slope failures and

debris flows triggered by Typhoon Lekima are mainly composed of Quaternary deposits, the influence of the bedrock lithology cannot be ignored, as the lithology variation commits to the differences of weathering and erosion (Bernard et al. 2019), which may

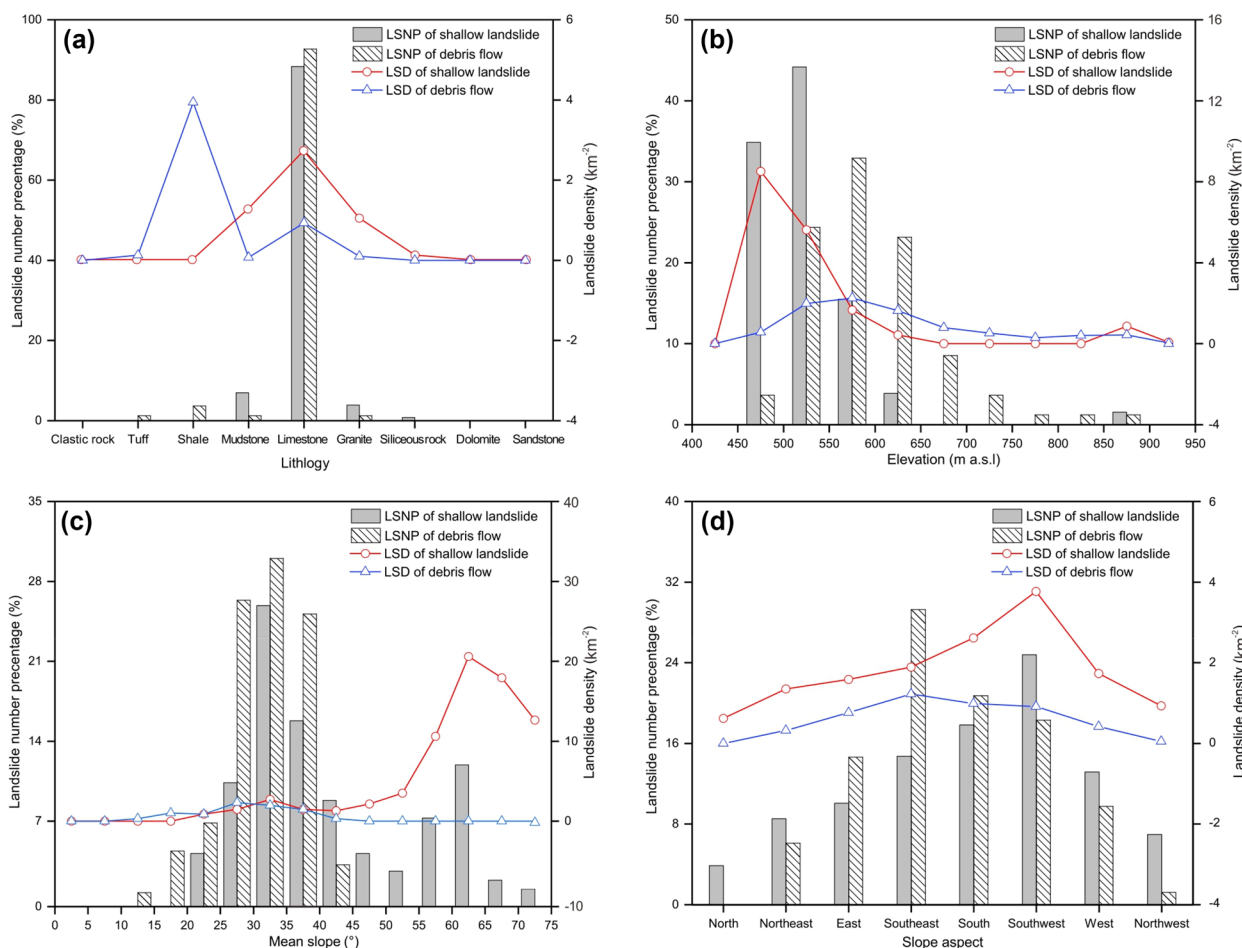


Fig. 8 Relationships between landslide distribution and geological and topographical parameters over the study area ((a) lithology, (b) elevation, (c) mean slope, (d) slope aspect)

further affect the formation of the original topography and cause slope deposits to possess various mechanical properties (Koons et al. 2012). In the study area, landslides that appeared in the limestone region account for the majority of the total occurrence, and the LSNP values for shallow landslides and debris flows are 88.0% and 92.7%, respectively (Fig. 8a). The corresponding LSD values of 2.7 km^{-2} and 0.9 km^{-2} also demonstrate the abundance of landslides. However, debris flows in the shale unit have a larger LSD (3.9 km^{-2}) than those in the limestone. This discordance between the maximum LSNP and LSD is correlated with the areal extension of the geological units. The limestone unit has 76 debris flows, which may be regarded as a relevant quantity in absolute terms, but if this amount is normalized according to the areal extension (81.8 km^2), the resulting LSD becomes lower than that of the shale unit. Conversely, only 3 debris flows occurred in the shale unit, but this low number corresponds to a very high density given the small area of 0.8 km^2 . Thus, it can be concluded that the shale unit is very prone to debris flows. This is consistent with the geological point of view because shale is a layered and very weak rock outcropping in hillsides where even a small slope gradient is enough to predispose the area to a high susceptibility of failure.

With different elevations, the LSNP and LSD values of shallow landslides and debris flows are summarized in Fig. 8b. The statistics indicate the largest possibility of the occurrence of shallow landslides, with elevations ranging from 450 to 550 m. In contrast, debris flows are easily placed at higher elevations ranging from 550 to 600 m. In terms of the mean slope, debris flows occupy the range of $10\text{--}45^\circ$, with a distribution close to normal, while shallow landslides

register a more widespread slope gradient from 20 to 75° (Fig. 8c). Moreover, the statistics suggest that mountains with slopes of $30\text{--}35^\circ$ are more prone to failure, with corresponding LSNP values for shallow landslides and debris flows of 27.1% and 30.5%, respectively. In addition, shallow landslides have a bimodal LSNP histogram and LSD curve compared with debris flows. As shown in Fig. 8c, except for the interval from 30 to 35° , shallow landslides have another slight aggregation ranging from 60 to 65° . To explain this phenomenon, an additional analysis for shallow landslides with slope angles larger than 55° was conducted. The results indicate that 84.4% of shallow instabilities were initiated from the excavated slope near roads or buildings, as shown in Fig. 6b. Thus, it can be concluded that the second increase in the LSNP for shallow translational slides is typically related to construction activities, which predispose steep slopes to landslide occurrence. Concerning the effect of the slope aspect on landslide distribution, unlike Typhoon Mangkhut (Abancó et al. 2021), slope failures caused by Typhoon Lekima do not have a distinct preponderant orientation. The LSNP histograms and LSD curve in Fig. 8d show that shallow landslides and debris flows mainly run towards the southeast, south, and southwest. This distribution is influenced by the spatial evolution of the typhoon, which moved from these directions (Figs. 2 and 3b) and by the spatial orientation of the mountainsides in the northern part of the area, where the occurrence of landslides was predominant (Fig. 5b).

Mobility of landslides

In addition to landslide distribution, another critical feature to consider in hazard analysis is landslide mobility, since different

Table 1 Geometrical parameters and apparent friction coefficients of landslides in the study area

Number	Vertical drop height H_{\max} (m)	Horizontal runout distance L_{\max} (m)	Area (m^2)	H_{\max}/L_{\max}	Type
1	3.5	5.2	2.7×10^1	0.7	Shallow landslide
2	5.3	9.1	7.4×10^1	0.6	Shallow landslide
3	7.6	10.7	7.7×10^1	0.7	Shallow landslide
4	6.8	9.9	1.2×10^2	0.7	Shallow landslide
5	6.5	13.7	1.3×10^2	0.5	Shallow landslide
6	8.1	19.2	2.1×10^2	0.4	Shallow landslide
7	14.1	22.7	2.4×10^2	0.6	Shallow landslide
8	13.7	33.2	4.0×10^2	0.4	Shallow landslide
9	32.5	58.4	9.1×10^2	0.6	Shallow landslide
10	71.4	121.6	2.4×10^3	0.6	Shallow landslide
11	56.0	153.3	0.3×10^4	0.4	Debris flow
12	165.7	598.9	4.3×10^4	0.3	Debris flow
13	160.4	477.4	6.1×10^4	0.3	Debris flow
14	156.3	560.1	13.6×10^4	0.3	Debris flow
15	351.0	1850.3	38.9×10^4	0.2	Debris flow

runout distances indicate different motion mechanisms and lead to different risk scenarios. Therefore, for emergency response and disaster mitigation, it may be necessary to understand the movement characteristics and scopes of instabilities influence. In this study, the apparent friction coefficient (Corominas 1996), which is defined as the ratio between the maximum vertical height (H_{max}) and the horizontal projection of the maximum travel distance (L_{max}), is employed to evaluate the mobility of some key landslides triggered by Typhoon Lekima. In this area, a total of 15 landslides with clearly distinguishable moving scars were measured during the field investigation, and the corresponding apparent friction coefficients are listed in Table 1. A low H_{max}/L_{max} value indicates that the landslide has high mobility, and vice versa. The H_{max}/L_{max} ratios vary from 0.2 to 0.7, with an average of 0.5 and with debris flows having higher mobility than shallow landslides, as expected.

Figure 9 compares the H_{max}/L_{max} values between landslides induced by Lekima and other landslide events worldwide. The mobility of landslides that occurred in the area affected by the 2008 Wenchuan earthquake (Fan et al. 2015) and the 2015 Gorkha earthquake (Dahlquist and West 2019) was smaller than that of landslides during Typhoon Lekima, while loess slides caused by irrigation (Peng et al. 2018) exhibited higher mobility than slope failures during Typhoon Lekima. In contrast, landslides triggered by extreme rainfall in Beijing in 2017 (Li et al. 2019), Medngdong in 2018 (Yang et al. 2020), and Puerto Rico in 2017 (Erin et al. 2020) seemed to have similar landslides mobilities to those in Doshi town, with the median H_{max}/L_{max} values of these four regional landslide

events ranging between 0.4 and 0.5 (group a–d in Fig. 9), suggesting that the rainfall amount might have some influence on landslide mobility.

Formation mechanism of debris flows

In this event, debris flows were more mobile than shallow landslides and typically travelled a long distance, so they were associated with a high energy level and a very high hazard level. A detailed investigation was conducted near the Wangzhuangwu catchment located in the southeastern part of the region (Fig. 10). At 17:00 CST on August 2019, a debris flow broke out in this drainage basin. The mixture of gravel soil, rock blocks, and muddy water rushed down the mountain and passed through the village downslope, destroying 4 houses and flooding more than 30 properties (Fig. 11).

The debris flow basin covers a catchment area of 0.9 km² and has an average width of 459.5 m. In terms of the topography, the southeast part is higher than the northwest, with a relative elevation difference of 351.1 m. To better understand the formation and movement features of the debris flow, the drainage basin is divided into two parts from top to bottom, as illustrated in Fig. 10. The upstream side is the area where debris flow originates and is transported. A mixture of water and particles migrated along mountain gullies and converged at the cross-section A–A'. Then, the debris flow crossed the channel confluence and entered the deposition area. Since the terrain is constricted in a narrow valley, the chaotic aggregation that travelled downslope had no other path; thus, it directly impacted the village (Fig. 11a, b). Field

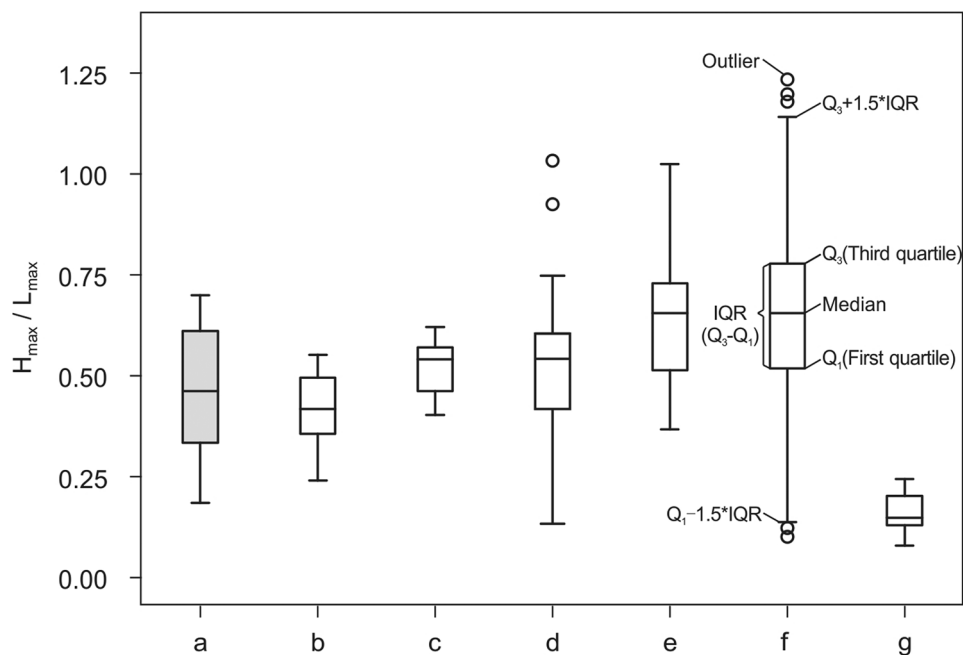
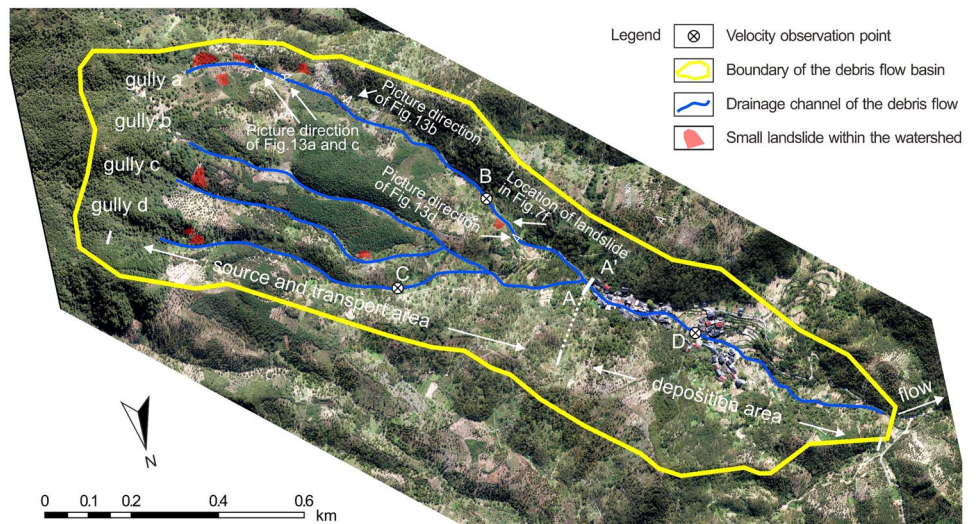


Fig. 9 Box plot distribution of worldwide apparent friction coefficients. ((a) Landslides during 2019 Super Typhoon Lekima, with a maximum rainfall intensity of 62.0 mm/h (this study); (b) rainfall-induced debris flows in Beijing, China, with a maximum rainfall intensity of 103.2 mm/h; (c) Rainfall-induced landslides and debris flows in Mengdong Town, China, with a maximum rainfall intensity of 97.4 mm/h; (d) debris slides and flows triggered by Hurricane

Maria in Puerto Rico, with a total rainfall of 508 mm in 72 h; (e) landslides induced by the 2008 Wenchuan earthquake, China; (f) post-seismic landslides associated with the 2015 Gorkha earthquake in Nepal; (g) Loess landslides in Shaanxi, China). Each box plot includes the interquartile range (IQR), median, and two outlier boundaries ($Q_1 - 1.5 \times IQR$ and $Q_3 + 1.5 \times IQR$, respectively). Empty circles indicate outliers

Fig. 10 Boundary of the basin influenced by debris flows



surveys have found plenty of evidence that rock fragments within muddy water scraped and hit structures (Fig. 11c, d). Eventually, the debris flow slowed down, and the variable clast content settled and accumulated in the vast farmland beyond the village. The relationship between the runup height (ΔH) and velocity (V_c) of a debris flow is estimated by Eq. (1), which simplifies the movement as a vertical upwards motion. In addition, the discharge of the debris flow (Q_c) can be determined by employing Eq. (2), where W_c is the cross-sectional area (Yang et al. 2020).

$$V_c = \sqrt{2g\Delta H} \quad (1)$$

$$Q_c = W_c V_c \quad (2)$$

Compared with observation point D, the mixture moved faster in the gullies a and d (points B and C), and the corresponding discharge was 16.2 m³/s, 61.1 m³/s, and 38.6 m³/s, respectively (Table 2). It is very likely that buildings settled in the runouts divided the debris flow and limited the motion. It should be stressed that before

Fig. 11 Field photos in the village that the debris flow passed through. ((a) Screenshot from the video taken by an eyewitness; (b) muddy trace on a building; (c) damaged housing along the pathway of the stream; (d) abrasion of a concrete column)



Table 2 Estimation of debris flow velocity and discharge in different observation points

Observation point	Runup height ΔH (m)	Cross-sectional area (m ²)	Velocity V_c (m/s)	Discharge Q_c (m ³ /s)
B	2.3	9.1	6.7	61.1
C	1.4	7.5	5.2	38.6
D	0.8	4.1	4.0	16.2

this event, no landslides or debris flows were reported to have damaged the village.

The abundance of solid material is critical to the formation of debris flows. In the Wangzhuangwu catchment, Quaternary sediments mainly originated from weathered Cambrian limestones and were susceptible to failure under heavy rainfall conditions. Meanwhile, the negative impact of land cover change cannot be ignored. Large-scale deforestation in the watershed reduced the reinforcement capability of root systems, predisposing them to the instability of soil cover (Masi et al. 2021). Therefore, during the typhoon event, gravel soil and rock blocks in the source and transport area were directly driven downslope by the surface runoff. In particular, some small landslides caused by rainfall infiltration also became the debris flow source as they accumulated in the drainage channel (Fig. 12a). On the other hand, the debris flow volume gradually increased during the runout due to extensive vertical and lateral erosion. Some noticeable scratches were found in the drainage channels (Fig. 12b). Moreover, the V-shaped channel in the source area changed to a U-shaped channel downstream (Fig. 12c, d).

Discussion

Because of climate change, extreme rainfall events are increasing in frequency, magnitude, and severity worldwide, and they are expected to have a significant impact on the occurrence of landslides (Emberson et al. 2021). To place the study of this event in a broader context, a comparison of the rainfall features from Typhoon Lekima with other typhoon-bound rainfall and abnormal precipitation events around the world is conducted, as exhibited in Fig. 13. Since the study area is far from the landfall location (Fig. 3a), the rainstorm here is relatively low and characterized by an average rainfall of 6.8 mm/h, which is smaller than the other 11 records. In addition, the maximum and total rainfall are also located at modest levels of approximately 62.0 mm/h and 300.5 mm, respectively. Even though the rainfall during Typhoon Lekima is situated at the lower-left corner of the scatter plot, the total and maximum daily precipitation reached the historical maximums for Daoshi Town since 1971. In other words, this is the first time that Daoshi Town has experienced such a catastrophic rainfall event. The rainfall infiltration changed the moisture content and further reduced the strength of the soil on the slope (Rosone et al. 2018). Consequently, a series of shallow landslides and debris flows occurred in the region, where few slope failures had occurred previously, corresponding to disastrous sediment discharge.

The detailed investigation provides an opportunity to offer insight into the analysis of the transformation pattern between shallow landslides and debris flows. Some scholars have explored that debris flows can originate from shallow landslides since the pore water pressure increases and liquefaction of the shear zone (Luna et al. 2012; Carey et al. 2021). In the study area, there are two other possible transformation patterns between landslides and debris flows, which are differentiated by their occurrence sequence. First, when landslides are deposited in the drainage channel before

Fig. 12 Field photographs showing the details of the Wangzhuangwu debris flow. ((a) Landslide deposits were carried away by the debris flow; (b) scratches left by the moving mixture; (c) V-shaped channel in the source area; (d) U-shaped channel downstream)

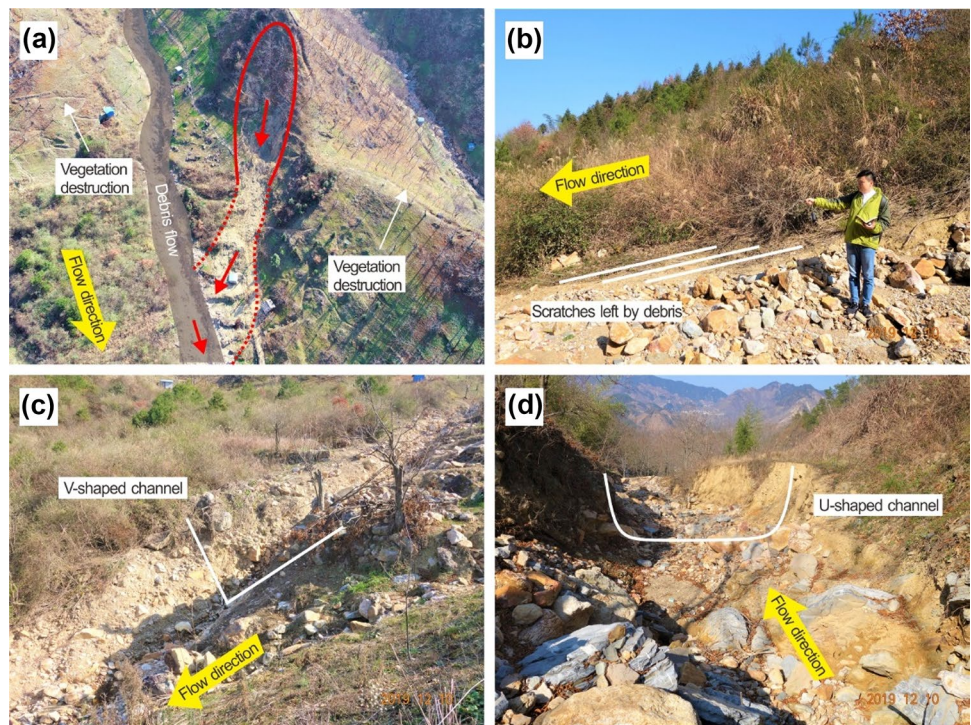
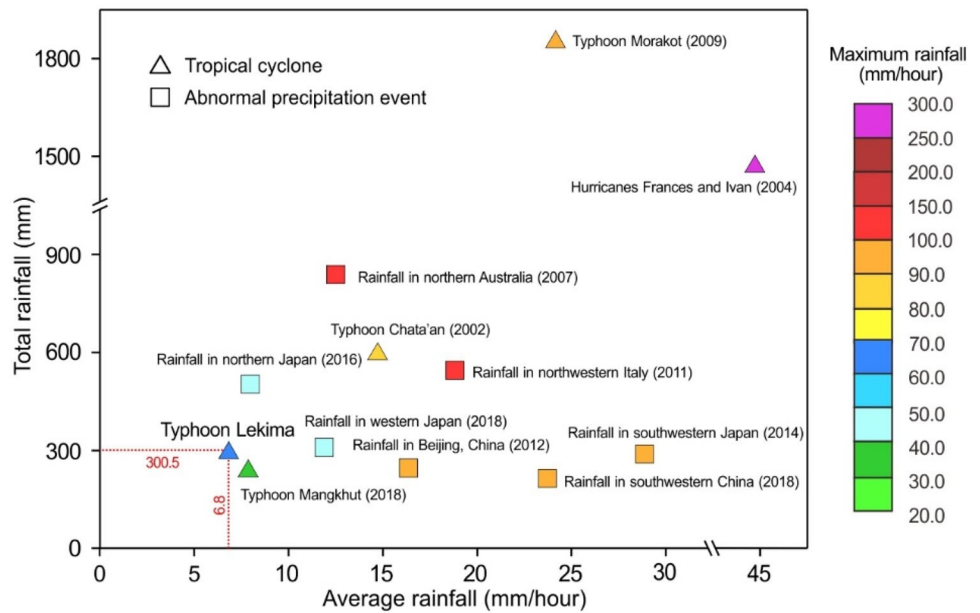


Fig. 13 Comparison of the rainfall parameters from Typhoon Lekima and other regional landslide events worldwide



or during the outbreak of a debris flow, the sediment is entrained and becomes a part of the mixtures, as illustrated in Fig. 14a. A typical example was found near the debris gully of the Wangzhuangwu watershed (Fig. 12a). The intersecting boundary of the shallow landslide with the drainage route and the disappearance of the toe of the accumulation indicated that the landslide occurred before the passage of the debris flow; then, the deposit was carried away by subsequent streamflow. Second, although debris flows cannot directly transform into landslides, the extensive erosion from streamflow is averse to the stability of the bank slopes (Fig. 6f). In some cases, these slopes may develop into landslide dams that lag behind debris flows and become a potential source of the subsequent mass movement (Figs. 6e and 14b). This kind of lagging effect has been widely reported in earthquake-affected areas, in which a great number of landslides are initiated a few years later after shaking stops (Fan et al. 2015; Dahlquist and West 2019). In this regard, a detailed investigation and inventory are critical and necessary.

To mitigate risk from landslides, countermeasures, such as population relocation, land use restriction, installation of

engineering structures (e.g., retaining walls, anti-piles, and drainage) and ground-based or remote sensing monitoring, are commonly used. However, given the high number of landslides in the wide area of the investigated site, one of the most cost-effective approaches is the establishment of the early warning system (EWS) (Piciullo et al. 2018). In our case, a preliminary analysis was performed to characterize the event that struck Daoshi town from the perspective of discussing the features needed for a site-specific EWS. The intensity-duration (I-D) threshold is a widely established criterion for regional landslide EWS, but its effectiveness is closely related to the technical characteristics of the system (Segoni et al. 2018; Abraham et al. 2020). As a consequence, the rainfall intensity of the triggering event was analysed to determine which time resolution is needed to effectively face similar events by an EWS based on rainfall thresholds. The most intense rainfall peak was taken into account, which was recorded starting from 16:00 CST on 10 August 2019, and the mean intensity recorded in all the time windows from 1 to 24 h was considered; then, those values were compared with some

Fig. 14 Diagrams showing the transformation between shallow landslides and debris flows

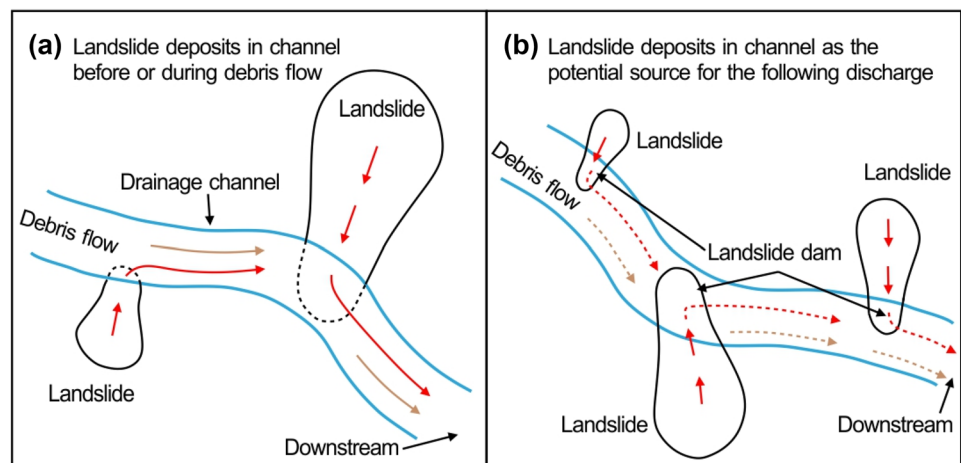
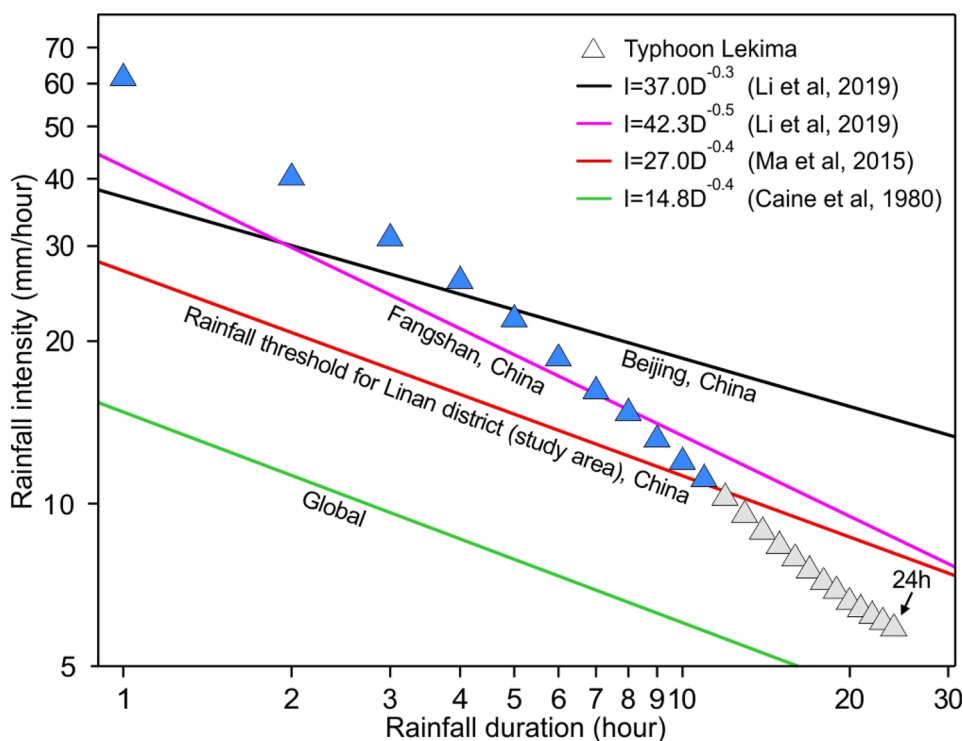


Fig. 15 Comparison between the extreme rainstorm of Typhoon Lekima and intensity-duration (I-D) thresholds from different regions



state-of-the-art I-D thresholds. Figure 15 shows that the rainfall event was well above the global threshold proposed by Caine (1980), but different outcomes were obtained considering site-specific thresholds. Indeed, the precipitation during the early 11 h exceeded the I-D threshold established for the Linan District, which is the upper-level territorial unit of the study area (Ma et al. 2015), while intensities calculated over wider time intervals fell below the triggering threshold. Moreover, rainfall intensities calculated from very short timespans are also greater than the critical rainfall defined for Beijing, China (less than 4 h), and Fangshan, China (less than 7 h) (Li et al. 2019). This outcome shows that the establishment of a site-specific EWS based on rainfall thresholds would be a potentially helpful tool to manage landslide risks in the area, but its actual effect would be conditioned by the time resolution of the rainfall measures and rainfall forecasts used. The analysis showed that considering daily or sub-daily (e.g., 12 h) rainfall data, the peak intensity would be missed, resulting in missed alarms. In other words, to better face similar events in the future, it is necessary to use modern rainfall measurements with at least hourly temporal resolution.

Conclusion

This study shows the joint impact of climate change and urban growth on a social system that until 2019 had been relatively safe from landslide hazards. The case study reported here is a preliminary investigation of the disastrous 10 August 2019 regional landslide event triggered by extreme rainfall from Typhoon Lekima in Daoshi Town, Zhejiang Province, China. The study area has had few historical landslide events and has never experienced similar precipitation before. To gain a comprehensive understanding of this event and provide basic data and understanding to address future

research activities, the spatial distributions, size characteristics, geological and topographical features, and mobility of different kinds of landslides were analysed.

A landslide inventory with 251 shallow landslides and 82 debris flows was compiled on the basis of field surveys and measurements. Most of them are concentrated in the north-central part of the study area and are relatively small in size. The mean areas for shallow landslide scars and debris flow basins are $3.2 \times 10^2 \text{ m}^2$ and $5.1 \times 10^4 \text{ m}^2$, respectively. The magnitude-frequency distribution of the shallow landslides has a characteristic rollover and tends to follow an empirical power law.

The main predisposing factors connected with the spatial distribution of landslide occurrence were identified to assist future studies on landslide susceptibility and better address territorial planning and reconstruction activities. The main drivers are lithology, elevation, slope gradient, and slope aspect; the typical intervals were identified, and connections with human activities were sometimes found, e.g., the slope gradient of shallow landslides shows a bimodal LSNP and LSD value distribution, and 32.4% of disasters are situated near structures.

Debris flows have higher mobilities than shallow landslides, and they can transform into each other with different occurrences. In detail, landslides can become a part of the debris mixture as they accumulate in the drainage channel before or during the streamflow burst. In addition, erosion from debris flows may also lead to landslide dams, which have the potential for mass movements in the future.

Finally, the peak intensity rainfall of the event was analysed and compared with the rainfall thresholds of the area, showing that to obtain effective warnings from similar events, the adoption of instruments and forecasts with fine (e.g., hourly) temporal resolution is mandatory.

This study characterizes a weather-induced landslide event that was unprecedented in the area and provides basic information and knowledge for risk mitigation. The collected data could also be used in future research activities, such as landslide susceptibility mapping, establishing an EWS, and developing mitigation and adaptation strategies.

Acknowledgements

This research is supported by the National Natural Science Foundation of China (No. 42172318). We wish to thank the Lin'an Branch, Hangzhou Administration of Planning and Natural Resources, Zhejiang Institute of Geological Survey Institute and Zhejiang Institute of Geological and Mineral Exploration for their assistance. We also thank the reviewers for their suggestions that improved the quality of this paper.

Declarations

Conflict of interest The authors declare no competing interests.

References

- Abancó C, Bennett G, Matthews A et al (2021) The role of geomorphology, rainfall and soil moisture in the occurrence of landslides triggered by 2018 Typhoon Mangkhut in the Philippines. *Nat Hazard Earth Sys* 21:1531–1550. <https://doi.org/10.5194/nhess-21-1531-2021>
- Abraham M, Satyam N, Kushal S et al (2020) Rainfall threshold estimation and landslide forecasting for Kalimpong, India Using SIGMA Model *Water* 12(4):1195. <https://doi.org/10.3390/w12041195>
- Bernard T, Sinclair H, Gailleton B et al (2019) Lithological control on the post-orogenic topography and erosion history of the Pyrenees. *Earth Planet Sc Lett* 518:53–66. <https://doi.org/10.1016/j.epsl.2019.04.034>
- Caine N (1980) The rainfall intensity-duration control of shallow landslides and debris flows. *Geogr Ann A* 62:23–27. <https://doi.org/10.1080/04353676.1980.11879996>
- Carey J, Cosgrove B, Norton K et al (2021) Debris flow-slide initiation mechanisms in fill slopes, Wellington, New Zealand. *Landslides* 18:2061–2072. <https://doi.org/10.1007/s10346-021-01624-6>
- Chen C (2016) Landslide and debris flow initiated characteristics after typhoon Morakot in Taiwan. *Landslides* 13(1):1–12. <https://doi.org/10.1007/s10346-015-0654-6>
- Corominas J (1996) The angle of reach as a mobility index for small and large landslides. *Can Geotech J* 33(2):260–271. <https://doi.org/10.1139/t96-005>
- Cruden D, Varnes D (1996) Landslide types and processes. In: Turner AK, Schuster RL (eds) *Landslides investigation and mitigation*. Transportation research board, US National Research Council. Special Report 247, Washington, DC, Chapter 3, pp. 36–75
- Cui Y, Jiang Y, Guo C (2019) Investigation of the initiation of shallow failure in widely graded loose soil slopes considering interstitial flow and surface runoff. *Landslides* 16:815–828. <https://doi.org/10.1007/s10346-018-01129-9>
- Dahlquist M, West A (2019) Initiation and runout of post-seismic debris flows: insights from the 2015 Gorkha earthquake. *Geophys Res Lett* 46(16):9658–9668. <https://doi.org/10.1029/2019gl083548>
- Easterling D, Meehl G, Parmesan C et al (2000) Climate extremes: observations, modeling, and impacts. *Science* 289(5487):2068–2074. <https://doi.org/10.1126/science.289.5487.2068>
- Eeckhaut M, Poesen J, Govers G et al (2007) Characteristics of the size distribution of recent and historical landslides in a populated hilly region. *Earth Planet Sc Lett* 256(3):588–603. <https://doi.org/10.1016/j.epsl.2007.01.040>
- Eker R, Aydın A, Hübl J (2018) Unmanned aerial vehicle (UAV)-based monitoring of a landslide: Gallenzerkogel landslide (Ybbs-Lower Austria) case study. *Environ Monit Assess* 190:28. <https://doi.org/10.1007/s10661-017-6402-8>
- Emberson R, Kirschbaum D, Stanley T (2021) Global connections between El Niño and landslide impacts. *Nature Commun* 12:2262. <https://doi.org/10.1038/s41467-021-22398-4>
- Erin K, Coe J, Schulz W et al (2020) Mobility characteristics of debris slides and flows triggered by Hurricane Maria in Puerto Rico. *Landslides* 17:2795–2809. <https://doi.org/10.1007/s10346-020-01445-z>
- Fan X, Leng X, Duan X (2015) Influence of topographical factors on movement distances of toe-type and turning-type landslides triggered by earthquake. *Rock Soil Mech* 36(5):1380–1388 (in Chinese)
- Fogarty E, Elsner J, Jagger T et al (2006) Variations in typhoon landfalls over China. *Adv Atmos Sci* 23(5):665–677. <https://doi.org/10.1007/s00376-006-0665-2>
- Guzzetti F, Malamud B, Turcotte D et al (2002) Power-law correlations of landslide areas in central Italy. *Earth Planet Sc Lett* 195(3–4):169–183. [https://doi.org/10.1016/S0012-821X\(01\)00589-1](https://doi.org/10.1016/S0012-821X(01)00589-1)
- Guzzetti F, Mondini A, Cardinali M et al (2012) Landslide inventory maps: new tools for an old problem. *Earth-Sci Rev* 112(1–2):42–66. <https://doi.org/10.1016/j.earscirev.2012.02.001>
- Hangzhou Municipal Bureau of Statistics (2017) *Hangzhou statistical yearbook 2017*. China Statistics Press, Beijing, p 2017
- Hungr O, Leroueil S, Picarelli L (2014) The Varnes classification of landslide types, an update. *Landslides* 11(2):167–194. <https://doi.org/10.1007/s10346-013-0436-y>
- Iverson R (2000) Landslide triggering by rain infiltration. *Water Resour Res* 36:1897–1910. <https://doi.org/10.1029/2000WR900090>
- Kang X, Xu G, Yu Z et al (2020) Experimental investigation of the interaction between water and shear-zone materials of a bedding landslide in the Three Gorges Reservoir Area. *China Bull Eng Geol Environ* 79:4079–4092. <https://doi.org/10.1007/s10064-020-01812-z>
- Kim J, Son K, Kim Y (2019) Assessing regional typhoon risk of disaster management by clustering typhoon paths. *Environ Dev Sustain* 21(5):2083–2096. <https://doi.org/10.1007/s10668-018-0086-2>
- Koons P, Upton P, Barker A (2012) The influence of mechanical properties on the link between tectonic and topographic evolution. *Geomorphology* 137(1):168–180. <https://doi.org/10.1016/j.geomorph.2010.11.012>
- Li Y, Ma C, Wang Y (2019) Landslides and debris flows caused by an extreme rainstorm on 21 July 2012 in mountains near Beijing. *China Bull Eng Geol Environ* 78(2):1265–1280. <https://doi.org/10.1007/s10064-017-1187-0>
- Liang X, Gui L, Wang W et al (2021) Characterizing the development pattern of a colluvial landslide based on long-term monitoring in the Three Gorges Reservoir. *Remote Sens* 13(2):224. <https://doi.org/10.3390/rs13020224>
- Liu X, Xie Z et al (2020) Analysis of rainstorm caused by super typhoon “Lekima” in Zhejiang Province of 2019. *J Meteorol Sci* 40(1):89–96 (in Chinese)
- Lou X, Ma H, Huang X et al (2020) Analysis on the causes of extreme precipitation by typhoon “Lekima” in Zhejiang Province. *J Meteorol Sci* 40(1):78–88 (in Chinese)
- Luna B, Remaître A, Van Asch T et al (2012) Analysis of debris flow behavior with a one dimensional run-out model incorporating entrainment. *Eng Geol* 128:63–75. <https://doi.org/10.1016/j.enggeo.2011.04.007>
- Ma T, Li C, Lu Z et al (2015) Rainfall intensity-duration thresholds for the initiation of landslides in Zhejiang Province, China. *Geomorphology* 245:193–206. <https://doi.org/10.1016/j.geomorph.2015.05.016>
- Masi E, Segoni S, Tofani V (2021) Root reinforcement in slope stability models: a review. *Geosci* 11(5):212. <https://doi.org/10.3390/geosciences11050212>
- Mok H, Lui W, Lau D et al (2020) Reconstruction of track and simulation of storm surge associated with the calamitous typhoon affecting the Pearl River Estuary in September 1874. *Clim past* 19:1–40. <https://doi.org/10.5194/cp-2019-36>
- Oouchi K, Yoshimura J, Yoshimura H et al (2006) Tropical cyclone climatology in a global-warming climate as simulated in a 20 km-mesh global atmospheric model: Frequency and wind intensity analyses. *J Meteorol Soc Jpn* 84(2):259–276. <https://doi.org/10.2151/jmsj.84.259>

- Peng J, Zhuang J, Wang G et al (2018) Liquefaction of loess landslides as a consequence of irrigation. *Q J Eng Geol Hydrogeol* 51(3):330–337. <https://doi.org/10.1144/qjegh2017-098>
- Piciullo L, Calvello M, Cepeda J (2018) Territorial Early Warning Systems for Rainfall-Induced Landslides *Earth-Sci Rev* 179:228–247. <https://doi.org/10.1016/j.earscirev.2018.02.013>
- Ren J (1991) On the Geotectonics of Southern China. *Acta Geologica Sinica (english Edition)* 4(2):11–136. <https://doi.org/10.1111/j.1755-6724.1991.mp4002001.x>
- Rosone M, Ziccarelli M, Ferrari A et al (2018) On the reactivation of a large landslide induced by rainfall in highly fissured clays. *Eng Geol* 235:20–38. <https://doi.org/10.1016/j.enggeo.2018.01.016>
- Rosi A, Tofani V, Tanteri L et al (2018) The new landslide inventory of Tuscany (Italy) updated with PS-InSAR: geomorphological features and landslide distribution. *Landslides* 15:5–19. <https://doi.org/10.1007/s10346-017-0861-4>
- Saito H, Korup O, Uchida T et al (2014) Rainfall conditions, typhoon frequency, and contemporary landslide erosion in Japan. *Geology* 42(11):999–1002. <https://doi.org/10.1130/G35680.1>
- Seboong O, Lu N (2015) Slope stability analysis under unsaturated conditions: case studies of rainfall-induced failure of cut slopes. *Eng Geol* 184:96–103. <https://doi.org/10.1016/j.enggeo.2014.11.007>
- Segoni S, Piciullo L, Gariano S (2018) A review of the recent literature on rainfall thresholds for landslide occurrence. *Landslides* 15:1483–1501. <https://doi.org/10.1007/s10346-018-0966-4>
- Wang G, Suemine A, Furuya G et al (2005) Rainstorm-induced landslides at Kisawa village, Tokushima Prefecture, Japan, August 2004. *landslides* 2(3):235–242. <https://doi.org/10.1007/s10346-005-0061-5>
- Webster P, Curry J, Liu J et al (2005) Changes in tropical cyclone number, duration, and intensity in a warming environment. *Science* 309(5742):1844–1846. <https://doi.org/10.1126/science.1121564>
- Wu C, Chen S, Feng Z (2014a) Formation, failure, and consequences of the Xiaolin landslide dam, triggered by extreme rainfall from Typhoon Morakot. *Taiwan Landslides* 11:357–367. <https://doi.org/10.1007/s10346-013-0394-4>
- Wu L, Wen Z, Huang R (2020) Tropical cyclones in a warming climate. *Sci China Earth Sci* 63(456–458). <https://doi.org/10.1007/s11430-019-9574-4>
- Wu Y, Chen L, Cheng C (2014b) GIS-based landslide hazard predicting system and its real-time test during a typhoon, Zhejiang Province. *Southeast China Eng Geol* 175(12):9–21. <https://doi.org/10.1016/j.enggeo.2014.03.005>
- Yang H, Yang T, Zhang S et al (2020) Rainfall-induced landslides and debris flows in Mengdong Town, Yunnan Province, China. *Landslides* 17:931–941. <https://doi.org/10.1007/s10346-019-01336-y>
- Zheng Z, Pan L, Qian Y et al (2021) Evolution characteristics of extreme heavy precipitation in coast of Zhejiang Province caused by Typhoon Lekima. *J Arid Meteorol* 39(2):269–278 (in Chinese)
-
- Supplementary information The online version contains supplementary material available at <https://doi.org/10.1007/s10346-022-01889-5>.
-
- Xin Liang · Kunlong Yin**
Faculty of Engineering, China University of Geosciences,
Wuhan 430074, China
- Samuele Segoni · Veronica Tofani · Nicola Casagli**
Department of Earth Sciences, University of Florence,
50121 Florence, Italy
- Juan Du** (✉) · **Bo Chai**
School of Environmental Studies, China University of Geosciences,
Wuhan 430074, China
Email: dujuan@cug.edu.cn